Cellular Outline Segmentation using Fractal Estimators

Adrián Salvatelli[1], José Caropresi[2], Claudio Delrieux[3], María F. Izaguirre[4] and Víctor Casco[4]

[1]Depto. de Bioingeniería, Grupo Inteligencia Artificial, Facultad de Ingeniería, Bioingeniería UNER, Ruta 11, K.10, Oro Verde, Entre Ríos, adrian.salvatelli@gmail.com.
[2]Depto. de Matemática e Informática, Facultad de Ingeniería, Bioingeniería UNER, Ruta 11, K.10, Oro Verde, Entre Ríos Depto. de Informática, FICH, UNL, Paraje El Pozo, Santa Fe, caropres@fich1.unl.edu.ar.

[3]DIEC, UNS, Av. Alem 1253, Bahía Blanca, claudio@acm.org (Partially funded by SECyT-UNS).

[4]Lab. Microscopía, Facultad de Ingeniería Bioingeniería, UNER, Ruta 11, K.10, Oro Verde, Entre Ríos vcasco@bioingenieria.edu.ar (Partially funded by PID: 6082-1).

ABSTRACT

Segmentation in biological images is essential for the determination of biological parameters that allow the construction of models of several biological problems. This helps to establish clear relationships between those models and the parameter estimation, and for elaboration of key experiments that give support to biological theories. Segmentation is the process of qualitative or quantitative information extraction (shape, texture, physical and geometric properties, among others). These quantities are needed to compute the biological descriptors for further classification (*v.g.*, cell counting, development stage assessment, and many others). This process is almost always supervised (*i.e.*, human assisted), since the quality of the images that are produced with classic microscopy technologies have defects that in general disallow the application of unsupervised segmentation techniques.

In this paper we investigate the use of the a local fractal dimension estimation as an image descriptor for microscopy images. This local descriptor appears to be robust enough to perform unsupervised or semisupervised segmentations, specifically in our study. We applied this technique on microscopy images of amphibian embryos' skin in which, using immunofluorescence techniques, we have labeled the cell adhesion molecule E-Cadherin. This molecule is one of the key factors of the Ca^{2+}-dependent cell—cell adhesion. Segmentation of the cellular outlines was performed using a processing workflow, which can be repeatedly applied to a set of similar images, from which information is extracted for characterization and eventual quantification purposes.

Keywords: Image Processing — Segmentation — Imunofluorescence Microscopy Images — Fractal Sets.

1. INTRODUCTION

Morphological techniques in cellular and molecular biology are aimed to understand both the complex cellular functions, and the interactions of the cells within the environment. To achieve this goal, it is indispensable to describe the location patterns of the significant molecules at a subcellular level. Fluorescence microscopy has been one of the most powerful molecule location tool since its inception in the early 1970s [7]. However, in cases where images correspond to thick specimens or dyed organisms *in toto* (as a whole), the quality of the results turn out to be degraded. For instance, images obtained by optical sectioning in fluorescence microscopy present diverse defects that render useless the application of unsupervised segmentation algorithms for classifying cellular forms and patterns. These defects include additive noise due to superimposition of optical stimuli, multiplicative noise due to imperfections in the molecule labeling process, blur due to progressive optical defocus, luminance fluctuations due to varying thickness in the specimen, and thermal and electronic noise in the sensor.

In this work we develop a processing workflow (*i.e.*, a sequence of processing steps) for the segmentation of cellular outlines in images obtained from specimens of the *Bufo arenarum*. In these specimens, molecules of cellular adhesion have been marked by immunofluorescence techniques, and therefore they exhibit most of the defects mentioned above. The workflow is based on computing the local fractal dimension as an image descriptor of the likelihood of a cellular outline being present in that part of the image. The local fractal dimension is estimated using the box counting algorithm (BFD). After this description step, adaptive filtering, border extraction, and geometric recognition techniques are applied. The results are satisfactory regarding the particular goal of determining the geometry of cellular membranes, and to be able to validate the specifically studied biological models. In addition, we show that the preliminary results of applying this workflow to other medical images (for example, ultrasound) are also satisfactory.

A summary of this paper is as follows. In the next Section we present the overall idea of fractal dimension in images, together with the local box fractal dimension method and the use of local fractal dimension for image segmentation. In Section 3 we introduce the workflow for unsupervised segmenta-

tion in immunofluorescence images. We elaborate on the techniques and present several examples. In the following Section we present the results of applying the workflow on the sample images, and also to different medical images. In Section 5 we present the conclusions and discuss the future work and further developments.

2. Local estimation of the box fractal dimension

In images, as well as in other non-deterministic sets, there is a direct relationship between the fractal dimension and the self-correlation coefficient of their characteristic function [10], [8]. This relationship suggests the possibility of computing an indirect estimation of the fractal dimension in sets of this kind[1] using statistical methods that extend the usual definitions of fractality. An example of this is Hausdorff dimension (or self-similarity dimension). A closed set A in an affine space is *self-similar* if A can be expressed as the union of $N(r)$ not overlapping copies of itself scaled with ratio r. In this case, the fractal dimension D of A is given by the relationship:

$$D = \lim_{r \to 0} \frac{\log(N(r))}{\log(\frac{1}{r})}. \quad (1)$$

The concept of self-similarity can be used to estimate the fractal dimension of an arbitrary set. Eq. 1 is the basis of the estimation of the fractal dimension of generalized sets in an abstract space. However, because its generality it is of little computational use. Several alternative methods are proposed in the literature to compute the fractal dimension of sets. In image processing, most of them are applied to previously binarized images.

One of the most popular computational methods is the box fractal dimension (BFD), which is based on measurements of the set over grids of variable size and position. In BFD, $N(r)$ is the amount of "visited cells" of radius r, and the regression is done in the logarithmic space of $\frac{\log(N(r))}{\log(1/r)}$. Given an image of $M \times M$ pixels, (which is previously binarized using Bayesian estimators for setting the threshold), we subdivide the image in grids of $s \times s$, where $M/2 \geq s > 1$ and $s \in Z$. Then, the space (x, y) is partitioned with cells of size s. In this case the radius is $r = s/M$. If some lit pixel of A is within a cell, we consider that the cell contributes to $N(r)$. The final value of $N(r)$, then, is obtained counting up all the cells of the grid that contained at least one lit pixel. $N(r)$ it is computed for different radii r, averaging the counts over grids superimposed in different positions of the image. Then, the fractal dimension D is estimated as the slope of the least squares regression that fits the scatter plot of $log(N(r))$ vs. $log(1/r)$ (see Fig. 1) [11].

[1] A binarized image can be regarded as the set of lit pixels in an affine subspace of $\Re^2$.

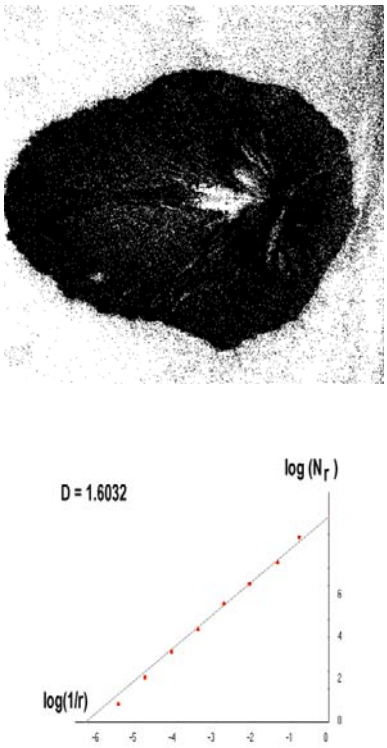

Fig. 1. (a) An input image, and (b) the least squares regression of the function $\frac{\log(N(r))}{\log(1/r)}$.

For establishing local estimations of D, it should be possible to find a similar slope along several orders of magnitude of r, which is not always possible. Therefore, for small M, the computed values for D are rough, provisional estimations. These values are not necessarily exact, but since they are precise enough, then they can be used as a local feature for image segmentation. The local BFD estimation proceeds taking a sub-image centered on the pixel to estimate. Sub-images of larger size produce better estimations, but also with a larger computational cost. In this paper we take grids of up to 7×7 pixels as good compromise between time and quality, which showed to be experimentally adequate in our examples.

The segmentation process can be understood as splitting foreground from background in an image [4]. If foreground and background have both different statistical distributions, they will have different fractals dimensions. Therefore, it would be possible to segment them apart in a suitable way using fractal descriptors, much better than with segmentation-based luminance thresholding. In Fig. 2(a) we represent the local BFD using a grayscale, where $D = 0$ corresponds to black and $D = 2$ to white. In Fig. 2(b) we show the histogram of the relative frequencies of D, together with three criteria of threshold choice (Euclidean, Bayesian, and minimal distance). In Fig. 2(c) we show the segmented image using the Bayesian discriminant as threshold.

In images in which border detection with convolution operators is not successful (with multiplicative

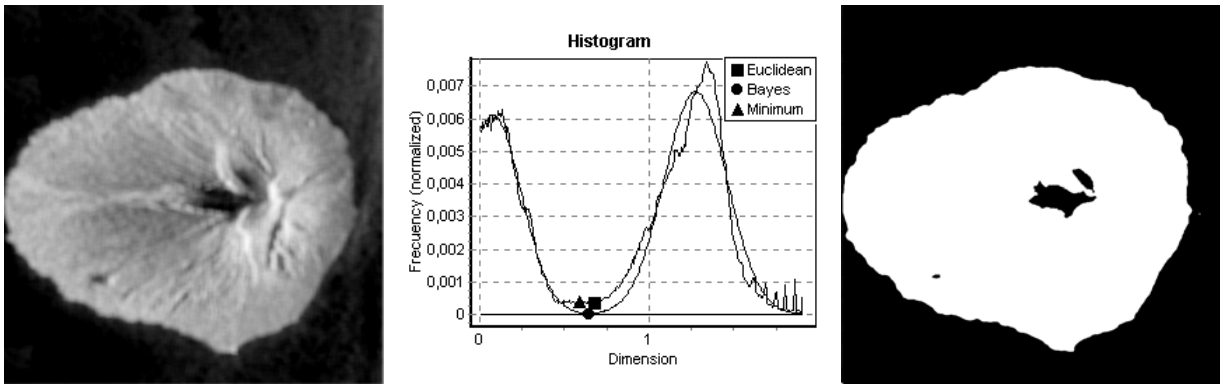

Fig. 2. (a) Local BFD D of the image in Fig. 1(a) (here represented as gray levels), (b) histogram of D and the thresholding values, and (c), binarization using the Bayesian classifier on D.

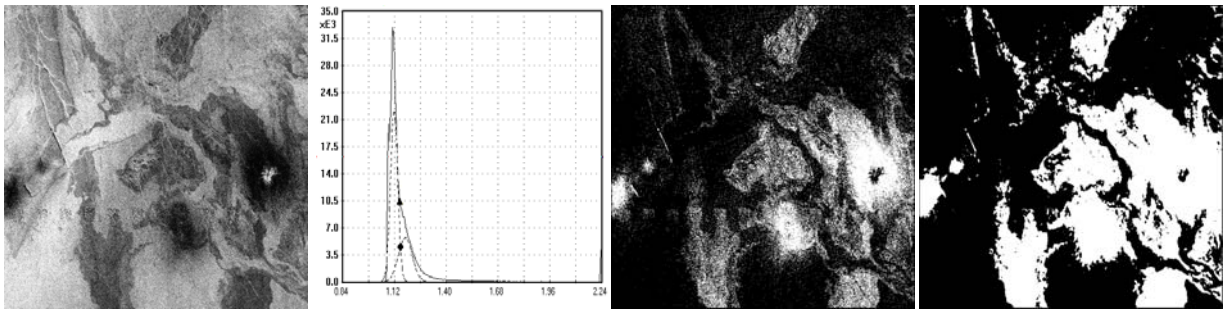

Fig. 3. (a) Input image, (b) histogram of its local BFD (unimodal), (c) luminance segmentation, and (d) BFD segmentation (in both cases, using Bayesian discriminant).

noise, defocused, with motion blur, etc.), this unsupervised segmentation strategy is robust, and produces adequate results [3]. However, when the histogram is not bimodal, a more refined analysis may be needed. Our underlying model of an unimodal, biased histogram, is to regard it as superimposition of two Gaussian distributions, with the foreground and background pixel intensities in each of them. However, since the means of the two distributions is too close, the resulting histogram is no longer bimodal. In this case, an adequate technique is to consider the bias towards one side of the overall histogram as due to the least populated class, which biases the distribution of the most populated class to one side. Fitting the biased side to the non-biased side (*i.e.*, making the distribution symmetric) amounts to subtract the influence of the least populated class to the whole histogram [2]. In this way the two underlying Gaussian distributions can be estimated and the segmentation threshold can be computed with the standard procedures, as shown in Fig. 3.

3. The processing workflow

In this section we describe the segmentation method by local fractal descriptors applied on the skin of *Bufo arenarum* embryos (stage 19) [5]. They were fixed in Carnoy solution, washed in `1X PBS` at room temperature and 0.1% `Triton X-100` (Sigma, St Louis) during 30 minutes at room temperature. After that they were incubated in normal goat serum 1:20 for 35 minutes, and then in rat anti-`E-Cadherin` monoclonal antibody (Transduction Laboratories, Lexintong, USA) 1:50 at 37°C for 75 minutes. After that, embryos were washed in `1X PBS` and then incubated in secondary antibody (`IgG-FICT` Sigma, St Louis, USA) 1:64 at room temperature for 105 minutes. Finally, the embryos were again washed in `1X PBS` and whole mounted using the anti-fading media Vectashield (Vector Laboratories Inc, Burlingame, CA, USA) to prevent the rapid fluorescence decay during microscopic examination.

The fluorescence images obtained by optical sectioning of these embryos exhibit several problems. First of all, the specimens do not have a uniform thickness, and then the image cannot be in focus everywhere. Different depth displacements change the position of the focused area in the tissue. Therefore, the information loss due to defocusing cannot be completely controlled. The image acquisition was produced with magnifications 40X and 100X, which give substantially different processing conditions. In Fig. 4 we show a group of images of the set to be processed, with different magnifications and depths. In general the 40X images exhibit more defocusing and information loss.

Second, the images have additive and digitalization noise introduced by the electronic acquisition system, and multiplicative noise due to the autofluorescence of the epithelial cell, which is a stochastic process

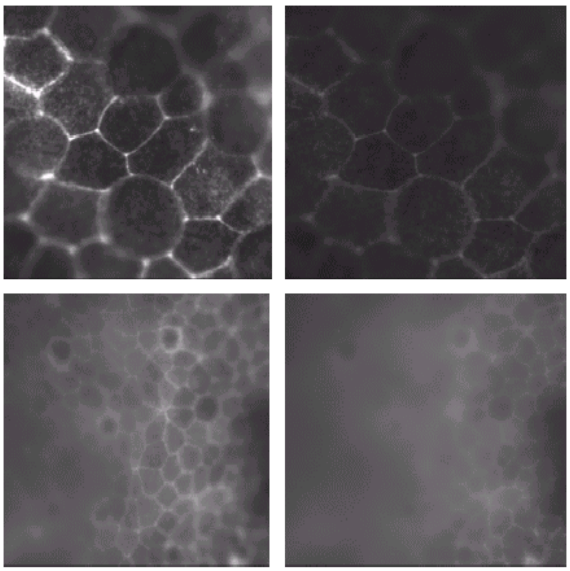

Fig. 4. Images of embryos of the *Bufo arenarun* produced by fluorescence microscopy of optical sectioning. (a) 100X magnification, first slice of the series. (b) 100X magnification, last slice. (c) 40X magnification, first slice. (d) 40X magnification, last slice.

that modulates the light emission phenomenon. The fluorocrome linked through the antibodies to the adhesion molecule `E-Cadherin` also can be bound to other, non specific molecules inside the cell. This creates multiple light sources that interfere with each other, producing the particular background noise that can be seen in Fig. 4. A third problem is due to the non uniformity of the fluorocrome binding and to the gradual loss of fluorescence emission. These two effects together produce local unevenness and changes in the light emission, and therefore in the intensity and contrast of the foreground in the image. Finally, the illumination is not uniform because the thickness of the tissue is not uniform either.

All these defects in the images determine that the usual segmentation methodologies will not be successful, either separately or together. In Fig. 5(a) we may appreciate the result of applying border detection to the image of the Fig. 4(a) after a median filtering (median filtering usually diminishes the sobresegmentation due to noise). In Fig. 5(b) we applied optimal Canny border extraction operator to the same image. Any further geometry recognition step to find the actual cell boundaries is very likely to fail. The cell boundary extraction problem in these images will require a more specific pipeline of processes. We will organize the workflow in three stages, image standardization and feature enhancement, boundary segmentation using border detection, and labeling and feature extraction. In this Section we will be concerned with the first two of these steps.

3.1 Image standardization and feature enhancement

Given the impossibility to detect borders in a straightforward way, we devised a processing method that

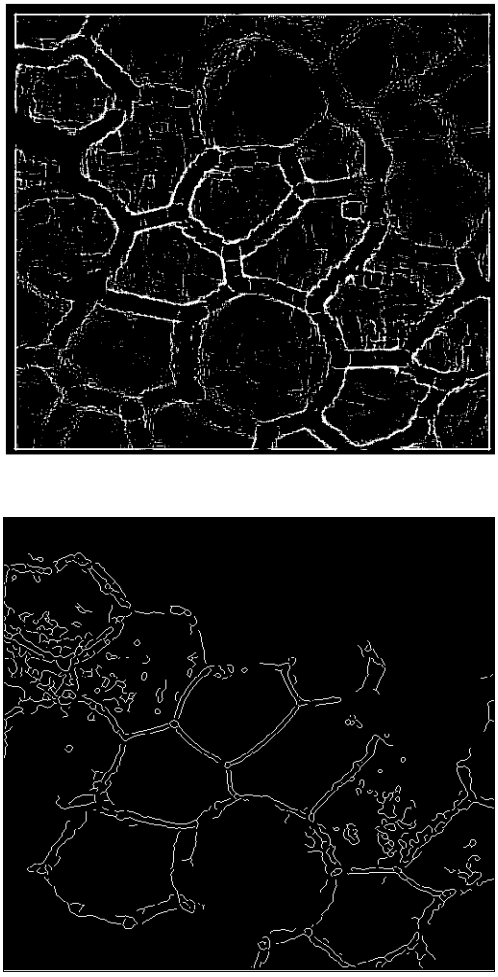

Fig. 5. (a) Border detection in Fig. 4(a) using border extraction after a median filtering, and (b) using the optimal Canny operator.

enhances the geometric local characteristics (specifically edges and vertices, which correspond with the cellular membrane and the adhesion molecules, respectively). The use of the BFD in this context turns out to be adequate for enhancing these features. The local BFD behaves robustly as an image descriptor even in the presence of all the defects in these images. In Fig. 6 we show the result of computing the local BFD on the image in Fig. 4(a) (and represented as a grayscale map) together with the histogram of the relative frequencies of the local BFD. We can see that this process filtered away the area with the most significant multiplicative noise (the area in focus), without altering the geometry and features of the boundaries in the defocused areas. A parameter in this step is the width of the window around a pixel where the BFD is being computed. In this example the width is set to 7×7.

To standardize the brightness of the BFD image, we apply an adaptive local equalization. This step takes subimages of 32×32 pixels, at each block it subtracts the minimum luminance, and then applies a uniform equalization. This provides a corrected luminance histogram without reducing the dynamic range or saturation. The next step is the supression

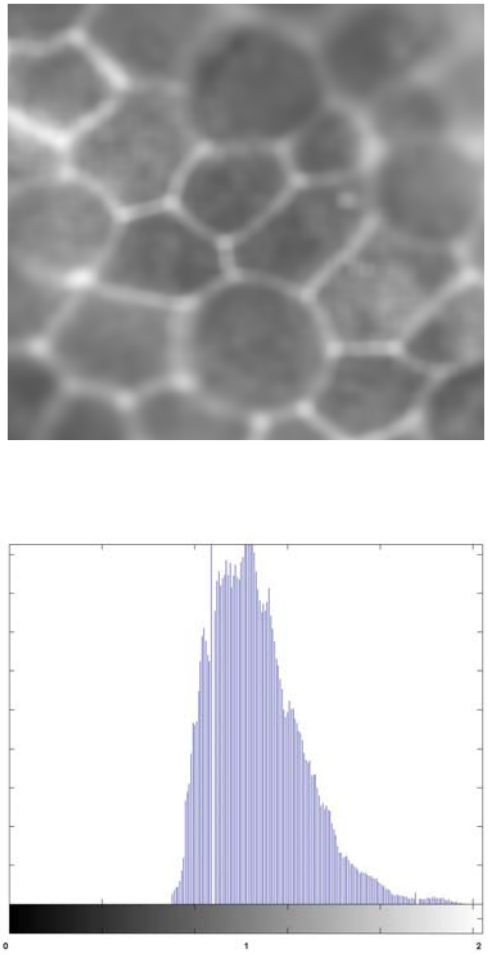

Fig. 6. (a) Local BFD of the image in Fig. 4 represented as a grayscale, and (b) the histogram of the corresponding BFD distribution.

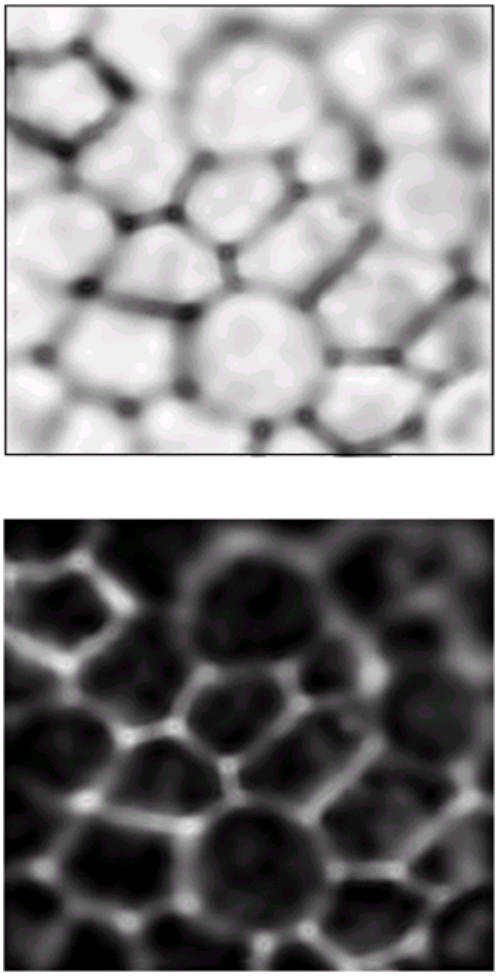

Fig. 7. (a) Image of Fig. 6(a) after luminance and contrast standardization, and (b) its negative image.

of additive noise, which can trigger undesired over-segmentation in the following stages. This noise is filtered using an adaptive Wiener filter of growing window width (10×10 up to 25×25), followed by a 20×20 median filter. Wiener filters have been proven adequate for noise reduction in optical images, where larger kernel sizes are used with larger magnifications, and the other way around. After these filtering, we enhance the contrast by means of grayscale gradient operators. We apply a nonlinear morphologic gradient enhancement which consists on the addition of the top hat operator followed by the subtraction of the bottom hat operator[2]. The structural element for these morphological operations is a disk, whose radius is also a parameter of the workflow. In Fig. 7 we can see the result of these processing steps. The next step (border extraction) will be processed using watershed (*i.e.*, finding the ridges of the basins of the minima). For this reason we generate also the negative of the resulting image.

[2]Top hat operator is the morphological gradient extraction *image minus eroded image*, and bottom hat is the complementary operator *dilated image minus original image*.

3.2 Border segmentation

The processing workflow will be unsupervised. So far all the steps in the enhancing and standardizing stage are unsupervised. Our purpose in this work is to provide the most complete and accurate geometric information of the cellular contours. This can be used in a further geometric recognition algorithm, which will be able to detect and characterize the tile patterns in cellular development. This extraction procedure should be automatic, providing a robust and adaptive performance even in the presence of blurred, non uniform and noisy boundaries. Unsupervised border extraction techniques are not well developed, and their performance in optical images is not well understood. We tested several of the available methods in the literature, among them active contours (snakes) [1], region growing [12], evolutionary algorithms [6], and morphological watershed [9]. This later technique was the one that produced the most adequate results.

As is well known in the literature, the performance of the watershed is very sensitive to the initialization process, which depends on the catchment basin implantation. Wrong implantation leads to over- or undersegmented images. Given the prior processing

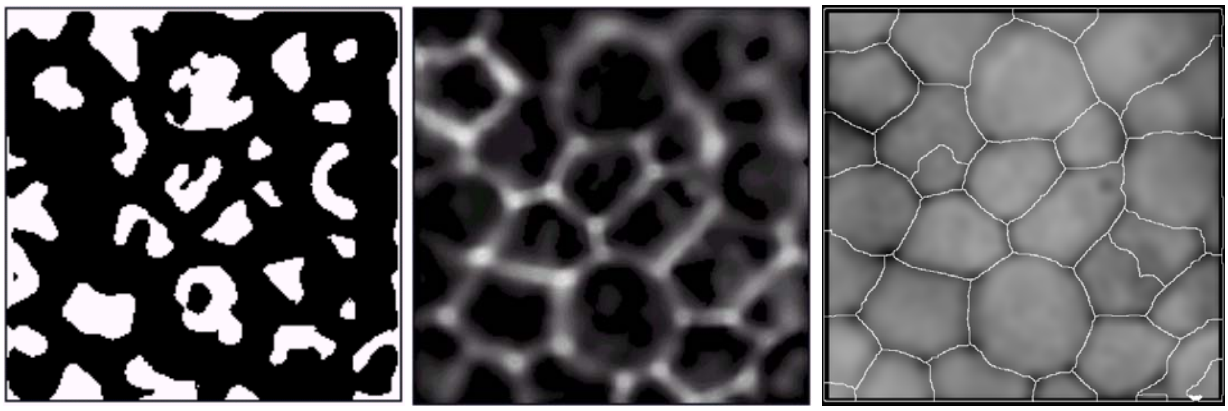

Fig. 8. (a) Catchment basin implantation on the image of Fig. 7(b), (b) extended minima, and (c) overlay of the borders segmented with the watershed over the image in Fig. 7(a).

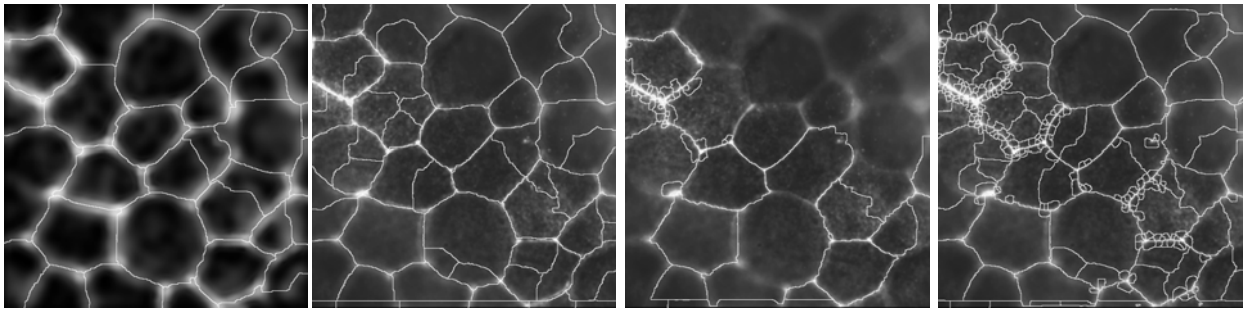

Fig. 9. (a) Segmentation of image in Fig. 4(b) with the complete workflow, (b) using only median filter 39×39, (c) using Wiener filter 20×20, and (d) using Wiener filter 25×25 .

in our images, the extended minima technique proves to be a successful catching basin implantation procedure. This technique finds local luminance minima, which are 8-connected components of size at least p pixels, whose luminance value is strictly lower than all the pixels of the boundary of the component. The extended minima technique finds all the local minima in the image. This set of minima can also be ordered with respect to the luminance difference with respect to the boundary. Then, a useful parameter for adjusting the segmentation is how many of the most important minima will be implanted as catchment basins. After the implantation process, the regions undergo a morphological flooding process until the basins divides are found. In Fig. 8 we show the results of applying this procedure to the image of Fig. 7(b).

4. Results and discussion

During the development of the processing workflow we tried several segmentation techniques, combinations thereof, and parameters settings. The whole process was tuned with the 100X images. The importance of the local BFD estimation can be seen in Fig. 9, where the results of withdrawing this step from the workflow are shown. The filtering + watershed process alone, at every possible parameter setting, always produced significant over- and undersegmentation. One of the advantages of this workflow is that it is flexible enough for adapting to different images, by means of the parameters that can be set prior to its application (i.e., the workflow is fixed and unsupervised, but can be tuned to the best performance in a particular case). With the 100X magnification images, the parameters used are: radius 3 for the structural element for top hat and bottom hat; 20 ± 2 size p of the connected elements for catchment basin implantation; Wiener filtering, with 10×10 kernel size; and a window of size 7×7 for the local BFD estimation. With the 40X magnification images, the results were also satisfactory, in this case with a 8 ± 1 size p for the catchment basis, no lowpass filtering, and the other parameters similar to the 100X magnification images (see Fig. 10).

As we already mentioned, the purpose of this paper is to develop a technique for unsupervised cellular outline segmentation in optical images. The next step is a geometrical pattern recognition procedure. This step identifies polygonal shapes and their adjacencies. Every closed polygonal shape is identified and labeled as a cell. The associated vertices, and therefore the amount of sides of the cell is the most important geometric characteristic. The vertices and edges are labeled, and therefore the adjacencies among cells are found. Other geometric descriptors computed over every cell are convex hull, area, Euler number, centroid, minimax box, equivalent and Feret diameters, perimeter, orientation, and eccentricity.

To test the applicability of this workflow in other contexts, we used it for feature segmentation in ultra-

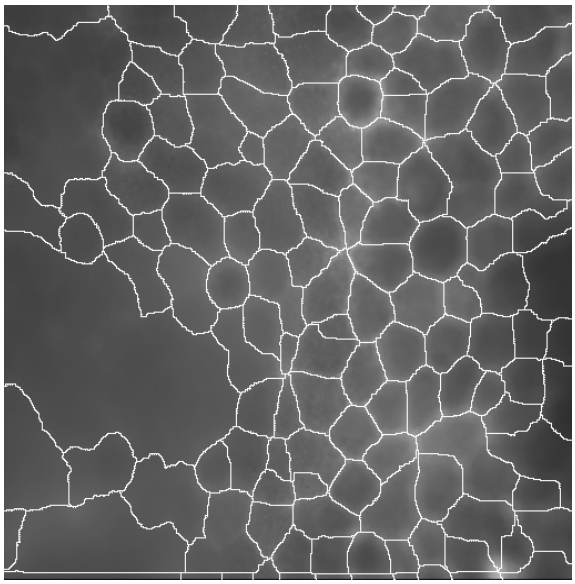

Fig. 10. The result of the workflow superimposed over the 40X magnification image in Fig. 4(c).

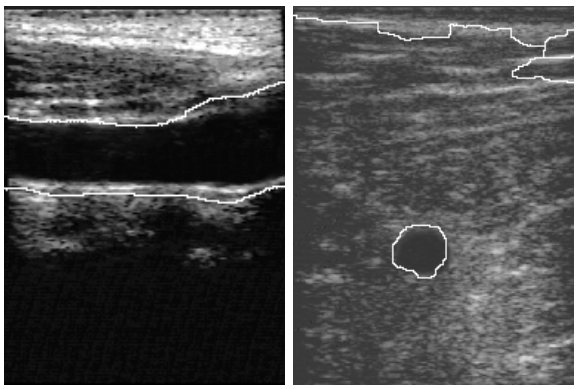

Fig. 11. The workflow applied to ultrasound images.

sound medical images, in particular to a transversal section of the femoral artery, and to a longitudinal section of the carotid. The results are very promising. In Fig. 11 we show the segmentation of the arteries, with very little oversegmentation.

5. Conclusion and future work

We presented a processing workflow for the unsupervised segmentation of cellular outlines in images of fluorescence microscopy of optical section obtained from biological specimens (embryos' skin of *Bufo arenarum*). These images present diverse defects that previously rendered useless the application of unsupervised segmentation algorithms for classifying cellular forms and patterns. These defects include additive noise due to superimposition of optical stimuli, multiplicative noise due to imperfections in the molecule labeling process, blur due to optical progressive defocus, luminance fluctuations due to varying thickness in the specimen, and thermal and electronic noise in the sensor. The workflow is based on using the local fractal dimension as an image descriptor of the likelihood of a cellular outline being present in that part of the image. Local fractal dimension is estimated using the box counting algorithm (BFD). After this description step, adaptive filtering, contouring, and geometric recognition techniques are applied.

The results obtained with 100X magnification images are satisfactory, and even with the 40X magnification images the results are adequate. The processed images allow the extraction of geometric information to determine the geometric patterns arisen in the cellular development. The only supervision that the workflow requires is to tune the processing parameter (kernel size, structural element radius, catchment basin implantation). We show that the preliminary results of applying this workflow to other medical images (for example, ultrasound) are also satisfactory.

We are currently working in further developments. The repeated application of the workflow over slices of 3D can be a good approach for feature segmentation in 3D images (PET, CAT, MRI) and also simulation models. Also, all the processing steps in the workflow are local, and therefore a GPU implementation might be able to process even large images in real time. Another interesting subject for research is to devise an intelligent procedure for tuning the parameters, probably based on cases or prior experience.

References

[1] A. Blake and M. Isard. *Active contours: the application of techniques from graphics, vision, control theory and statistics to visual tracking of shapes in motion*. Springer-Verlag, 1998.

[2] C. Delrieux and R. Katz. Hybrid image recognition architecture. In *SPIE's 16th Annual International Symposium on Aerospace/Defense Sensing, Simulation, and Controls*, Florida USA, 2002. SPIE-The International Society for Optical Engineering.

[3] C. Delrieux and R. Katz. Image Segmentation Through Automatic Fractal Dimension Classification. In *Argentine Symposium on Computing Technology*, Buenos Aires, 2003. 32 JAIIO, Jornadas Argentinas de Informática e Investigación Operativa,.

[4] Rafael González and Richard Woods. *Digital Image Processing*. Addison-Wesley, Wilmington, USA, 1996.

[5] K.L. Gosner. A Simplified Table for Staging Anuran Embryos and Larvae. *Herpetologica*, 16:183–190, 1960.

[6] R. Katz and C. Delrieux. Boundary Extraction Through Gradient-Based Evolutionary Algorithm. *Journal of Computer Science and Technology*, 3:7–12, 2003.

[7] Adams C. L., Chen Y. T., Smith S. J., and Nelson W. J. Mechanisms of Epithelial Cell-Cell Adhesion and Cell Compaction Revealed by High-resolution Tracking of E-Cadherin-Green Fluorescent Protein. *The Journal of Cell Biology*, 142(4), 1998.

[8] B. Mandelbrot and J. van Ness. Fractional Brownian Motion, fractional noises and applications. *SIAM Review*, 10(4):422–437, 1968.

[9] J. Park and J. M. Keller. Snakes on the Watershed. *IEEE Transactions on Pattern Analysis and Machine Intelligence*, 23(10):1201–1205, 2001.

[10] H.-O. Peitgen and D. Saupe. *The Science of Fractal Images*. Springer-Verlag, New York, 1986.

[11] J. C. Russ. *The Image Processing Handbook*. CRC Press, Boca Raton, FL, 1989.

[12] C. Xu and J. L. Prince. Snakes, Shapes, and Gradient Vector Flow,. *IEEE Transactions on Image Processing*, 28(3):359–369, 1998.